MONTANA STATE UNIVERSITY

Angle-resolved photoemission study of the antimony:allium arsenide interface using synchrotron radiation

by James Russell Myron

A thesis submitted in partial fulfillment of the requirements for the degree of Doctor of Philosophy in Physics
Montana State University
© Copyright by James Russell Myron (1988)

Abstract:
The electronic properties of the overlayer-semiconductor interface system GaAs(110)+Sb(0),p(lxl) where 0 = 1/2-2 ML, are studied with synchrotron radiation-based polarization -dependent angle-resolved ultra-violet photoemission spectroscopy (PARUPS).

Two core level effects are reported, Sb-4d core binding energy shifts and the Sb-4d threshold effect. The binding energy shifts of the Sb-4d core are analyzed with curve fitting procedures and indicate the existence of two inequivalent Sb bonding sites, one on Ga and the other on As. The antimony core threshold effect is observed in angle-resolved constant final energy spectroscopy (ARCFS), photoemission yield spectroscopy, and electron energy loss spectroscopy data at energies of 32.5 and 33.75 eV. This is an Auger decay mechanism (non-excitonic) which involves the Sb-4d core and an empty Sb-derived surface state S7'. The energy of S7' is inferred to be 1.18 eV above the valence band maximum (VBM).

Valence band measurements were performed with normal emission EDC and ARCFS spectra. Transitions before and after Sb evaporation were mapped onto the theoretical energy bands. A phenomenon, the characteristic amplitude effect, is reported wherein bulk band transition amplitudes are changed by the ordered monolayer. The effect is independent of light polarization, but dependents on the initial states. Evidence for non-uniform band shifting is seen in EDC spectra for hv = 60 eV where the surface contribution to photoemission is more dominant. In the ARCFS study, a new GaAs+Sb interface state S4' 3 eV below the VBM, is identified for A\MP and A\\MP. The Sb-derived surface state S5 near the VBM is observed. A GaAs surface state M2, detected at the M-point, is located 1.8 eV below the VBM. Bulk band state B3 has initial state in valence band 2 and shows the same characteristic amplitude effect which was studied at normal emission.

ANGLE-RESOLVED PHOTOEMISSION STUDY OF THE ANTIMONY:GALLIUM ARSENIDE INTERFACE USING SYNCHROTRON RADIATION

by

James Russell Myron

A thesis submitted in partial fulfillment
of the requirements for the degree

of

Doctor of Philosophy

in

Physics

MONTANA STATE UNIVERSITY
Bozeman, Montana

June 1988

(C) COPYRIGHT

by

James Russell Myron

1988

All Rights Reserved

D378
M9976

APPROVAL

of a thesis submitted by

James Russell Myron

This thesis has been read by each member of the thesis committee and has been found to be satisfactory regarding content, English usage, format, citations, bibliographic style, and consistency, and is ready for submission to the College of Graduate Studies.

7/7/88
Date

Gerald A. Lopeyre
Chairperson, Graduate Committee

Approved for the Major Department

7/8/88
Date

Robert J. Stevens
Head, Major Department

Approved for the College of Graduate Studies

July 8, 1988
Date

Henry L. Parsons
Graduate Dean

STATEMENT OF PERMISSION TO USE

In presenting this thesis in partial fulfillment of the requirements for a doctoral degree at Montana State University, I agree that the Library shall make it available to borrowers under the rules of the Library. I further agree that copying of this thesis is allowable only for scholarly purposes, consistent with "fair use" as prescribed in the U.S. Copyright Law. Requests for extensive copying or reproduction of this thesis should be referred to University Microfilms International, 300 North Zeeb Road, Ann Arbor, Michigan 48106, to whom I have granted "the exclusive right to reproduce and distribute copies of the dissertation in and from microfilm and the right to reproduce and distribute by abstract in any format."

Signature 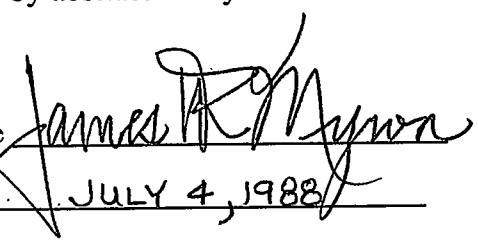

Date JULY 4, 1988

This thesis is dedicated in memory of my father, Russell "Babe" Gordon Myron. His encouragement and interest in my education was a positive force from grade school through graduate school. While I was growing up, Babe would often take on all the farm chores, in order to permit me to work on my lessons. As a successful Montana farmer, his perseverance and aspiration to excellence in his endeavors were a trademark. I strived for these ideals throughout the long process of measurement, analysis, and study. My only regret is that he is not here for the thesis completion. But somehow, I feel, he knows its done.

VITA

James Russell Myron was born in Sidney, Montana on November 21, 1952, the son of Russell Gordon and Doris Bodil Myron. He has an older brother, Gordon, and two sisters, Patricia and Cheryl.

Jim attended elementary school at a two-room rural school in the small farming community of Crane, Montana. Later he graduated as Valedictorian of the Class of 1971 from nearby Sidney Senior High School. Summers and weekends were spent helping on the family farm near Crane in the Lower Yellowstone Valley throughout high school and undergraduate school years. He started college at Montana State University in September 1971. A Bachelor of Science degree in physics was obtained in June of 1976 and a B.S. degree in mathematics was received the following year. 1975 was spent touring Europe. After starting graduate school at M.S.U. in January, 1978, he joined Dr. G.J. Lapeyre's photoemission research group. A Master of Science degree was obtained in physics in June of 1980.

The summers of 1981 and 1982 were spent working on special geophysical projects for Amoco Production Company of Houston, Texas. Also in 1982, he was co-investigator on a Department of Energy Appropriate Technology Grant in Bozeman. The remaining time was devoted to thesis measurements at the Synchrotron Radiation Center near Madison, Wisconsin.

In September of 1983 he took a permanent position with Amoco in Houston and is presently involved in finding and evaluating new science and technology in the exploration of oil and gas. Data reduction, analysis, and thesis writing was done in absentia while also working for Amoco.

ACKNOWLEDGMENTS

I am particularly grateful for the guidance and support of my thesis advisor, Dr. Gerald J. Lapeyre. His knowledge and intuition in surface physics was a valuable asset to my training. Also much appreciation is extended to Dr. James R. Anderson for giving important on-site advice at the Synchrotron Radiation Center near Madison, Wisconsin during the many months of data collection. He is truly an experimentalist, par excellence and it was an honor to learn under him. Dr. John Hermanson and Rolan Allen (Texas A & M University) gave important theoretical insight on many occasions, which I appreciate.

Thanks goes to the many others who contributed to the new photoemission system, including Dr. Dick Smith, Gwyn Williams, Franco Cerrina, Recep Avci, Franz Stucki, Peter Zurcher, as well as Mark Baldwin, Tony Knick, and Al Beldering at M.S.U., and the staff at the University of Wisconsin's SRC and PSL.

Several people gave me help during the arduous four year analysis and writing phase in Houston. Special thanks go to my colleague Stefan F. Nowina for his enthusiastic help and fine humor. For help with the manuscript, I owe a lot to Susan Metzler, Bubba Townsend, and a special friend, Jane Price.

Long overdue gratitude is extended to Mr. Knut Hoversten, an excellent teacher, who showed me the scientific pathway many years ago. Finally, words cannot fully convey the appreciation I have for my family's support over the years while doing my graduate work. Gordon, Patti, Cheryl, and Mom truly understood how important the Ph.D. was to me.

TABLE OF CONTENTS

1. STATEMENT OF THE PROBLEM 1

2. INTRODUCTION 2

3. THEORY OF PHOTOEMISSION 5

The Photoemission Process 7
Experimental Aspects 8
Three-step Model of Photoemission 12
Three Modes of Photoemission 20
Conservation of Photoelectron Momentum 25
The One-step Model of Photoemission 29
Relationship Between Experiment Parameters and Theory 38

4. PREVIOUS STUDIES 43

5. EXPERIMENTAL EQUIPMENT AND PROCEDURES 51

Synchrotron Radiation Center 51
Electron Storage Ring - Tantalus II 52
Monochromators 54
Main Experimental Chamber 56
Chamber Design 60
Ultra-high Vacuum Pumping 62
Light Optics (Mirror Box) 62
Sample Manipulator and Holder 65
Sample Cleaving Equipment 69
Antimony Evaporator Equipment 69
LEED and AES Systems 73
ELS System 73
Electron Energy Analyzers 76
Plane Mirror Analyzers 77
Cylindrical-mirror Analyzers 80
Twin-axis Goniometer 81
Data Acquisition Electronics 84
Pulse Counting Electronics 84
Sample Preparation 87
Clean Sample Preparations 87
Overlayer Sample Preparations 88

6. CORE LEVEL MEASUREMENTS 92

High Resolution Core Lineshape Study 95
Lineshape Fitting of Sb-4d Core 97
Results 101

TABLE OF CONTENTS - CONTINUED

Page

Core and Surface State Interaction Study 102
Theory of Recombination 105
Photoemission Yield Spectra 108
ELS 110
Results 114

7. ELECTRONIC STRUCTURE MEASUREMENTS 115

Normal Emission EDC Study 118
Experimental Approach 118
Data Processing and Reduction 118
Determination of Perpendicular Wavevector 119
Data and Analysis 127
Comparison of Sb and Ge overlayers on GaAs(110) 156
High Energy Normal Emission EDCs 162
Results 165
Constant Final Energy Spectroscopic (CFS) Study 167
Experimental Consideration 167
Data Processing 168
Data and Analysis 169
Results 176

8. SUMMARY 185

REFERENCES CITED 191

APPENDICES 197

Appendix A: Normal Emission EDC data Polarization angle 0 198
Appendix B: Normal Emission EDC data Polarization angle 180 217

LIST OF TABLES

Table Page

1. Three Modes of Photoemission 23
2. Symmetry elements in BZ and SBZ for GaAs(110) 39
3. Bonding geometry of GaAs(110)+Sb 46
4. Theoretical surface states for GaAs(110)+Sb (Bertoni *et al.*) 48
5. Theoretical surface states for GaAs(110)+Sb (Mailhoit *et al.*) 49
6. Antimony Overlayer Calibration Data 91
7. Binding energies for Ga-3d, Sb-4d, and As-3d cores 93
8. Surface-related states at M(Ga) and X'(Ga) 179

LIST OF FIGURES

Figure Page

1. Surface analytical spectroscopies used in this work 6
2. Generalized concept of photoelectron spectroscopy 9
3. The three-step model of photoemission 14
4. The universal escape curve 19
5. The photoemission surface for a hypothetical solid 22
6. Electron momentum crossing the crystal/vacuum interface 27
7. Comparison of a photoemission experiment to LEED experiment 32
8. Wave function decomposition in LEED versus photoemission 33
9. Bulk-like, band-gap, and surface-like photoemission 36
10. Surface and bulk Brillouin Zone for GaAs(110) 41
11. Surface Brillouin Zone for GaAs(110) 42
12. Overlayer-induced electronic states on III-V semiconductors 45
13. Atomic structure of GaAs(110)+Sb(1 ML),p(1x1) 47
14. Experimental layout at the Synchrotron Radiation Center 53
15. One-meter Seya-Namioka monochromator 55
16. Three-meter toroidal grating monochromator 57
17. Schematic of the photoemission system 59
18. Main experimental chamber for photoemission 61
19. Ultra-high vacuum pumping configuration 63
20. Typical pump-down curve 64
21. GaAs sample holder (perspective view) 66
22. GaAs sample holder with heater (cross section) 67
23. Setup for antimony evaporation for overlayer growth 70
24. Typical antimony evaporation curve 72
25. Schematic of the electronics setup for AES and ELS 74
26. Plane Mirror Analyzer (3-d schematic) 78
27. Schematic of PMA and twin-axis goniometer 82
28. Block diagram of photoemission acquisition electronics 85
29. Ratio of core amplitudes versus Sb dosage 90
30. EDC spectra showing Ga-3d, Sb-4d, and As-3d cores 94
31. High-resolution EDC spectra of the Sb-4d core 96
32. Antimony core levels with Lorentzian line fits 98
33. ARCFS spectra showing Sb core threshold effects 103
34. The energetics of core hole decay mechanisms 106
35. Polarization-dependent photoemission yield spectra 109
36. Sb core threshold effect shown in ELS data 111
37. Data processing of normal emission EDC data 120
38. Theoretical structure plot for GaAs(110) for initial band #2 122
39. Theoretical structure plot for GaAs(110) for initial band #3 123
40. Theoretical structure plot for GaAs(110) for initial band #4 124
41. Experimental structure plot for GaAs(110), pol. 90 126
42. Experimental structure plot for GaAs(110)+Sb(0.6ML), pol. 90 128
43. EDC difference spectra, transition A, pol. 90, hv=10-22 eV 130
44. EDC difference spectra, transition A, pol. 90, hv=22-30 eV 131
45. Energy bands of experiment and theory, transition A, pol. 90 132

TABLE OF FIGURES - CONTINUED

Figure Page

46. Peak amplitudes of transition A versus light polarization 134
47. EDC difference spectra, transition B, pol. 90, hv=10-22 eV 136
48. EDC difference spectra, transition B, pol. 90, hv=22-30 eV 137
49. Energy bands of experiment and theory, transition B, pol. 90 138
50. Peak amplitudes of transition B versus light polarization 139
51. EDC difference spectra, transition C, pol. 90, hv=10-22 eV 142
52. EDC difference spectra, transition C, pol. 90, hv=22-30 eV 143
53. Energy bands of experiment and theory, transition C, pol. 90 144
54. EDC difference spectra, transition D, pol. 90, hv=10-22 eV 145
55. EDC difference spectra, transition D, pol. 90, hv=22-30 eV 146
56. Energy bands of experiment and theory, transition D, pol. 90 147
57. EDC difference spectra, transition E, pol. 90, hv=10-22 eV 150
58. Energy bands of experiment and theory, transition E, pol. 90 151
59. EDC difference spectra, transition F, pol. 90, hv=10-22 eV 152
60. Energy bands of experiment and theory, transition F, pol. 90 153
61. Sb and Ge overlayers on GaAs for polarization 90, hv = 15 eV 157
62. Sb and Ge overlayers on GaAs for polarization 90, hv = 18 eV 158
63. Sb and Ge overlayers on GaAs for polarization 0, hv = 15 eV 160
64. Sb and Ge overlayers on GaAs for polarization 0, hv = 18 eV 161
65. High energy normal emission EDC spectra 163
66. Stainless steel Seya light curves 170
67. Light curve corrections applied to CFS data 171
68. ARCFS spectra at M (Ga) and pol. 0 for GaAs(110) + Sb(0.6 ML)..... 172
69. ARCFS spectra at M (Ga) and pol. 90 for GaAs(110) + Sb(0.8 ML)..... 173
70. ARCFS spectra at X'(Ga) and pol. 0 for GaAs(110)+Sb(0.6 ML) 174
71. ARCFS spectra at X'(Ga) and pol. 90 for GaAs(110)+Sb(0.5 ML) 175
72. Surface state located on theoretical energy band diagram 177
73. Experimental structure plot for GaAs(110), pol. 0 199
74. Experimental structure plot for GaAs(110)+Sb(0.6ML), pol. 0 200
75. EDC difference spectra, transition A, pol. 0, hv=10-22 eV 201
76. EDC difference spectra, transition A, pol. 0, hv=22-26 eV 202
77. Energy bands of experiment and theory, transition A, pol. 0 203
78. EDC difference spectra, transition B, pol. 0, hv=10-22 eV 204
79. EDC difference spectra, transition B, pol. 0, hv=22-26 eV 205
80. Energy bands of experiment and theory, transition B, pol. 0 206
81. EDC difference spectra, transition C, pol. 0, hv=10-22 eV 207
82. Energy bands of experiment and theory, transition C, pol. 0 208
83. EDC difference spectra, transition D, pol. 0, hv=10-22 eV 209
84. EDC difference spectra, transition D, pol. 0, hv=22-30 eV 210
85. Energy bands of experiment and theory, transition D, pol. 0 211
86. EDC difference spectra, transition E, pol. 0, hv=10-22 eV 212
87. EDC difference spectra, transition E, pol. 0, hv=22-26 eV 213
88. Energy bands of experiment and theory, transition E, pol. 0 214

TABLE OF FIGURES - CONTINUED

Figure Page

89. EDC difference spectra, transition F, pol. 0, hv=10-22 eV 215
90. Energy bands of experiment and theory, transition F, pol. 0 216
91. Experimental structure plot for GaAs(110), pol. 180 218
92. Experimental structure plot for GaAs(110)+Sb(0.6ML), pol. 180 219
93. EDC difference spectra, transition A, pol. 180, hv=10-22 eV 220
94. EDC difference spectra, transition A, pol. 180, hv=22-30 eV 221
95. Energy bands of experiment and theory, transition A, pol. 180 222
96. EDC difference spectra, transition B, pol. 180, hv=10-22 eV 223
97. EDC difference spectra, transition B, pol. 180, hv=22-30 eV 224
98. Energy bands experiment and theory, transition B, pol. 180 225
99. EDC difference spectra, transition C, pol. 180, hv=10-22 eV 226
100. EDC difference spectra, transition C, pol. 180, hv=22-30 eV 227
101. Energy bands experiment and theory, transition C, pol. 180 228
102. EDC difference spectra, transition D, pol. 180, hv=10-22 eV 229
103. EDC difference spectra, transition D, pol. 180, hv=22-30 eV 230
104. Energy bands of experiment and theory, transition D, pol. 180 231
105. EDC difference spectra, transition E, pol. 180, hv=10-22 eV 232
106. EDC difference spectra, transition E, pol. 180, hv=22-30 eV 233
107. Energy bands of experiment and theory, transition E, pol. 180 234
108. EDC difference spectra, transition F, pol. 180, hv=10-22 eV 235
109. EDC difference spectra, transition F, pol. 180, hv=22-30 eV 236
110. Energy bands of experiment and theory, transition F, pol. 180 237

ABSTRACT

The electronic properties of the overlayer-semiconductor interface system GaAs(110)+Sb(θ),p(1x1) where θ = 1/2-2 ML, are studied with synchrotron radiation-based polarization -dependent angle-resolved ultra-violet photoemission spectroscopy (PARUPS).

Two core level effects are reported, Sb-4d core binding energy shifts and the Sb-4d threshold effect. The binding energy shifts of the Sb-4d core are analyzed with curve fitting procedures and indicate the existence of two inequivalent Sb bonding sites, one on Ga and the other on As. The antimony core threshold effect is observed in angle-resolved constant final energy spectroscopy (ARCFS), photoemission yield spectroscopy, and electron energy loss spectroscopy data at energies of 32.5 and 33.75 eV. This is an Auger decay mechanism (non-excitonic) which involves the Sb-4d core and an empty Sb-derived surface state S_7'. The energy of S_7' is inferred to be 1.18 eV above the valence band maximum (VBM).

Valence band measurements were performed with normal emission EDC and ARCFS spectra. Transitions before and after Sb evaporation were mapped onto the theoretical energy bands. A phenomenon, the characteristic amplitude effect, is reported wherein bulk band transition amplitudes are changed by the ordered monolayer. The effect is independent of light polarization, but dependents on the initial states. Evidence for non-uniform band shifting is seen in EDC spectra for $h\nu = 60$ eV where the surface contribution to photoemission is more dominant. In the ARCFS study, a new GaAs+Sb interface state S_4, 3 eV below the VBM, is identified for $A \perp MP$ and $A // MP$. The Sb-derived surface state S_5 near the VBM is observed. A GaAs surface state M_2, detected at the $\overline{M}$-point, is located 1.8 eV below the VBM. Bulk band state B_3 has initial state in valence band 2 and shows the same characteristic amplitude effect which was studied at normal emission.

CHAPTER 1

STATEMENT OF THE PROBLEM

In its most general form, the thesis problem was to understand better the properties of ordered overlayer-semiconductor interfaces by investigation of a specific model system. This model system should possess the ideal interface properties of junction abruptness, chemical stability, and structural order.

It would be necessary to prepare this interface reliably and measure its electronic properties *in situ*, with polarization-dependent angle-resolved ultra-violet photoemission spectroscopy (PARUPS) using synchrotron radiation. Of principal importance would be identification of overlayer-induced interface states. Characterization of these states would allow an experimental check on existing theoretical calculations. However, general exploration of any interface associated phenomena would be valuable in furthering our understanding of these interfaces, including core electron and bulk electron behavior.

In order to study the model interface system adequately, completion of the design and construction of an new photoemission experimental system with advanced PARUPS capabilities would be necessary.

CHAPTER 2

INTRODUCTION

> "During the last thirty-five years much experimental evidence has been brought to bear upon the phenomenon that a large current will pass in one direction and small current, if any at all, in the opposite direction, through contacts of certain dissimilar solids." (Hartsough 1914).

This quotation refers to the rectification effect, which lay at the heart of the theory of metal-semiconductor (MS) interfaces. The MS interface was the principal focus of this thesis. Several MS theories have been proposed over the years (Schottky 1939, Bardeen 1947, and Brillson 1982), however today no single theory correctly predicts the complete behavior of even simple interfaces.

Even though interface related work has been done for over one hundred years, the study and characterization of solid state interface systems is currently a rapidly growing field of surface science. The basic research community has investigated the surface and bulk properties of clean crystalline materials for the last several years and they are generally regarded as understood (Weaver 1986). We are now in a good position to take the next logical step; examination of the bonding region between dissimilar materials - the interface. For basic science, it affords the opportunity to extend many ideas, including chemisorption on semiconductors, semi-classical junction models, and band bending theories (Dalven 1980). For applied science and microelectronics, the importance cannot be overstated. Within this decade, the characteristic gate size of electronic

integrated circuits will move into the submicron regime and as the surface to volume ratio of gates becomes larger, interface effects will play a significant role in device performance (Harris 1984).

For compound semiconductors, the chemical and electrical behavior at MS interfaces is very complex (Brillson, 1982) and often occurs over large microscopic distances (tens of angstroms) as opposed to an abrupt interface. The metal atoms can interact strongly with the clean semiconductor to produce two chemically distinct regions with varying properties. First, the reaction region is where new metal-cation or metal-anion bonds are formed. And second, the interdiffusion region is caused by either an outdiffusion of semiconductor atoms through the metal (*e.g.*, InAs(110)+Au) or metallic indiffusion (*e.g.*, GaAs(110)+Au) towards the semiconductor.

According to Brillson, it is the chemical reactivity of the metal with the semiconductor which governs, through interdiffusion, the interface thickness. Empirically, the stronger the metal-anion bonding, the more abrupt will be the interface.

Finding a good model system without the complications noted above was desirable in order to study the fundamental interactions occurring at the interface. The interface system chosen was the cleaved (110)-face of gallium arsenide GaAs, with overlayers (1/2-2 ML) of antimony Sb, deposited at room temperature. This system, GaAs(110)+Sb,p(1x1), was a good model system for the following reasons:

(1) GaAs(110) is a well understood and technologically important material. (Blakemore 1987, Ferry 1985).

(2) Sb grows as an ordered, epitaxial overlayer at room temperature on cleaved GaAs(110) (Skeath 1982 p.13).

(3) GaAs(110)+Sb forms an abrupt interface with little diffusion of Sb into the bulk or Ga/As out to the surface region, which is not the case for many other metal-GaAs systems (Lin *et al.* 1987)

(4) The surface unit net is preserved in size and mirror symmetry when going from GaAs, *as-cleaved* to the overlayer system.

(5) The antimony on the surface is in a single crystal phase and resists oxidation compared to GaAs, *as-cleaved*, since the new surface has no unsatisfied bonds.

(6) Multiple layers of antimony will thermally desorb for temperatures between 250° C and 350° C (Carelli and Kahn 1982).

(8) Important theoretical calculations of the electronic structure have been performed by Bertoni *et al.* (1983) and Mailhoit *et al.* (1985).

CHAPTER 3

THEORY OF PHOTOEMISSION

Several surface analytical measurement techniques were used in the course of investigations of GaAs(110)+Sb. Figure 1 schematically defines these various techniques and indicates the general characteristics of each.

At the top is Ultra-violet Photoemission Spectroscopy (UPS), which is a subclass of Photoemission Spectroscopy (PES) where the incident particle is a photon ($h\nu = 10$ to 100 eV). It is a highly surface sensitive method with an investigation depth of 5 to 18 Å (1-3 ML). By conservation of energy, the photoelectron ejected from the sample has a energy equal to the photon energy reduced by the binding energy E_b of the electron when it was in a bound state and by the work function ϕ of the sample.

The second technique in Figure 1 is Electron Loss Spectroscopy (ELS) which uses a low kinetic energy incident electron (50-100 eV) as the incident particle and measures the energy of the emitted electrons. These spectra have an elastic peak, composed of the electrons which undergo elastic Coulomb scattering, and a wide variety of energy loss features due to plasmons (collective charge excitations), Auger transitions, and other inelastic processes. We employed ELS first as a nondestructive technique to quantify the thickness of the antimony overlayers which were evaporated onto the GaAs crystal. Latter, ELS was found to reveal new effects which could be related to the formation of the overlayer. These new effects which were revealed in the ELS data will be discussed in the section on the antimony core threshold studies (Chapter 6).

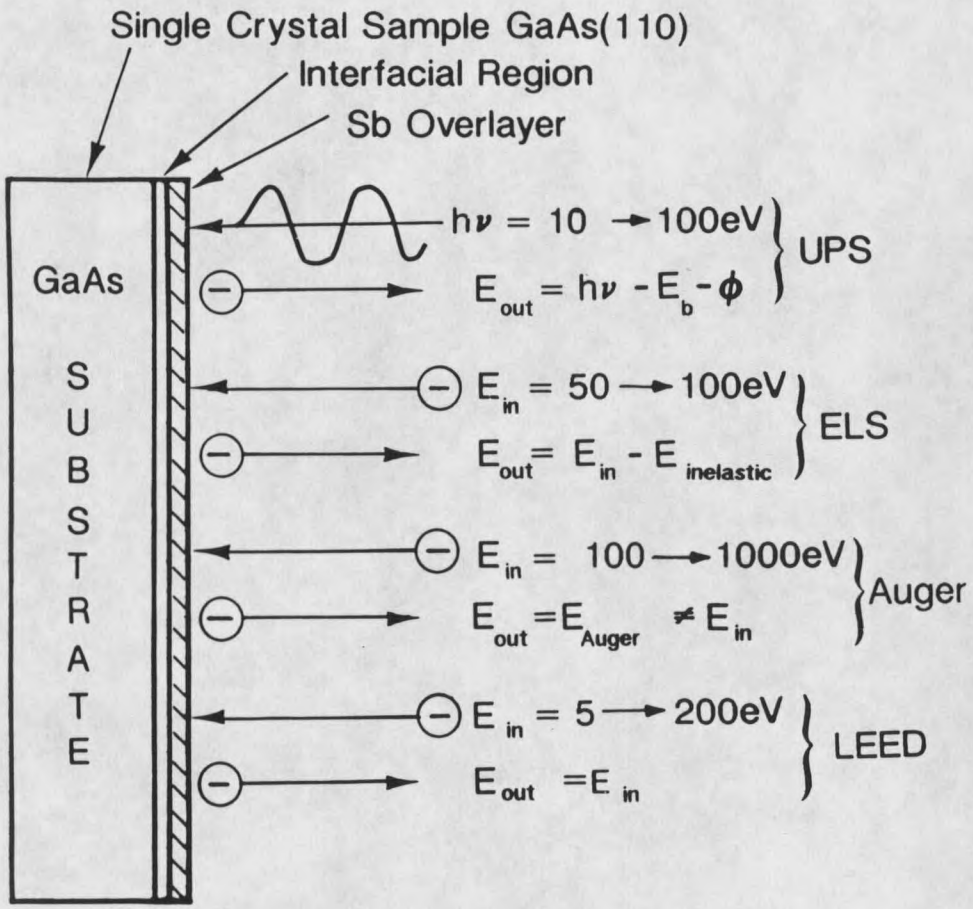

Figure 1. Surface analytical spectroscopies used in this work. The output particle of each technique is an electron of kinetic energy E_{out}. The input "probe" particle is either a photon of energy $h\nu$ (UPS) or an electron of energy E_{in}.

Auger Electron Spectroscopy (AES) was the third technique used. The basis for AES is a nonradiative transition where a vacancy (caused by ionization by an incident particle) in an inner shell of an atom is filled via the two-electron Auger process. Here an electron fills the vacancy and releases a characteristic amount of energy to a correlated electron (the Auger electron). Subsequently, this Auger electron is ejected from the sample with a unique energy E_{Auger} related to the binding energies of the atomic orbitals involved in the process. The Auger transition energy is rather like a unique chemical "fingerprint". At low kinetic energies (100 eV) the technique is very surface sensitive, since a low-energy Auger electron can escape only from the first few sample layers. Although AES has quantitative capabilities (Carlson 1975, Feldman and Mayer 1986), it was only used in this work when the overlayer sample could be sacrificed, since Zurcher (1982) had reported electron beam damage in GaAs(110)+Ge samples.

The last technique, Low Energy Electron Diffraction (LEED), was used routinely to characterize the sample surface before and after overlayer growth and to orient the symmetry axis of the crystal. LEED relies on elastic scattering and diffraction of slow electrons (50-200 eV) to determine the surface net and therefore the surface order. Of all these techniques, UPS was the principal method employed in this research work and will be the subject of the remainder of this chapter.

The Photoemission Process

Photoemission has a rich heritage in the physics community. The photoelectric effect was discovered by Hertz in 1887 (Weidner *et al.* 1968). An explanation of the effect, which postulated the quantization of light, was proposed by Einstein in 1905. Later, Millikan, through careful experimentation, verified Einstein's theory of the

photon, and constructed one of the first photoemission systems (Trigg 1975). Today the effect is exploited as a powerful spectroscopic technique for studying the quantum properties of solids. Spicer (1982) gives a interesting account of the role photoemission has played in the development of surface science.

A closely related research field to PES is the optical properties of solids (Wooten 1972) where the optical reflectance of a sample is measured as a function of the photon energy $h\nu$ of the incident light. The optical spectra manifest excitation processes within the material, but photoemission is more specific since it examines the electrons which have escaped from the sample as a result of irradiation by monochromatic light. Therefore PES, unlike optical reflectivity, gives the final state energy of the excitation as well as the excitation energy, which is of importance in understanding the electronic and optical properties of solid materials.

Experimental Aspects

Consider an arrangement as shown in Figure 2. Light (photons) impinges on the surface in a direction (θ_I,ϕ_I), with energy $h\nu$ and polarization given by the vector potential $\vec{A}$. The photoelectron ejected into the vacuum travels in a direction (θ_P,ϕ_P) with a kinetic energy E_k and momentum $\vec{p}$ towards the detector.

The detector acts as a directional kinetic energy bandpass filter. The energy passband is termed the detector's energy window. By scanning the energy window and keeping a fixed direction, a histogram of the number of photoelectrons at each kinetic energy value, called an Angle-Resolved Energy Distribution Curve (AREDC) results. A hypothetical EDC is shown in Figure 2, and is composed of several parts:

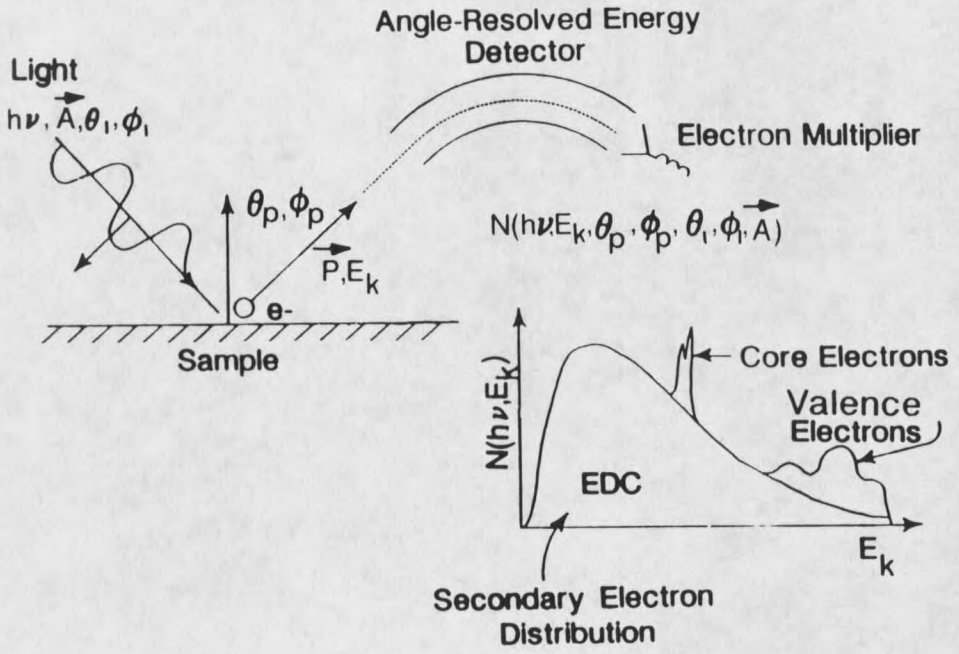

Figure 2. Generalized concept of photoelectron spectroscopy. Shining light onto the sample produces photoemitted electrons which are energy analyzed by the angle-resolving detector, resulting in an EDC.

(1) The secondary electron distribution (SED) is a broad background curve with a long decaying tail resulting from inelastic scattering of the photoelectrons within the sample (Caroli 1973). Generally, this background is subtracted from the EDC in preliminary processing. These electrons are amongst the slowest-velocity electrons in the EDC and, because of their rather featureless nature, they are not of interest to us here.

(2) The core electron peaks are rather sharp features which result from electrons excited from deep core states. These core states are the tightly bound inner electronic shells of the atom. The studies presented in Chapter 6 pertain to interface related effects manifested in the core states.

(3) The valence electron features manifest the electronic bonding or band structure of the material and directly reveal the behavior of the solid; in this case, the interface system. These states are very sensitive to the many acquisition parameters of the experiment. When the detector is moved to a new analysis angle, the valence features will generally change and in the case of GaAs, the changes will often be dramatic, since the band structure is complex . Chapter 7 will cover several experiments which were designed to study these features.

Photoemission spectroscopy is inherently very rich in information. The purpose of much of the effort in a photoemission experiment is to define and measure the many parameters. The photocurrent J is a function of at least ten parameters, most of them related to the source and detector configuration:

$$J = J(h\nu,\theta_A,\phi_A,\theta_I,\phi_I;E_k,\theta_P,\phi_P,s;X) \qquad (1)$$

where

the source parameters are:

photon energy: $h\nu$.

polar angle of the light's vector potential, $\vec{A}$: θ_A .

azimuthal angle of the light's vector potential, $\vec{A}$: ϕ_A .

polar angle of the light's propagation direction: θ_I .

azimuthal angle of the light's propagation direction: ϕ_I .

the detector parameters are:

kinetic energy of the photoelectrons: E_k.

polar angle of the photoelectron's momentum vector, $\vec{p}$: θ_P .

azimuthal angle of the photoelectron's momentum vector, $\vec{p}$: ϕ_P .

Lastly, the sample parameters are:

The photoelectron's spin polarization s, which we will ignore, and a manifold of sample characteristics which complicate the method. They have been lumped under the X factor. These include the type of material, crystal face, sample preparation, and surface cleanliness. Careful experimental technique is of paramount importance here in order to characterize the system.

Experimentally, we fix all the acquisition parameters (source and detector),usually adjusting only the photon energy $h\nu$ and scanning the kinetic energy E_k. This is the angle-resolved energy distribution curve (AREDC) mode of photoemission, resulting in a curve like shown in Figure 2. With this AREDC data (angle-resolved and energy-analyzed photocurrent), we try to determine the properties of the material. Using theoretical

models of photoemission as a basis (*e.g.* the three-step model) coupled possibly with theoretical calculations of the electronic structure of the system, we relate the data back to properties and excitation mechanisms of the material. In particular, our goal is to understand better the nature of the Ga-Sb and As-Sb bonding and how it relates to properties of the GaAs+Sb interfacial region.

Up to now we have only talked about the empirical aspects of photoemission, namely, measuring the kinetic energy and momentum of photoemitted electron after light has irradiated a material. A conceptual and theoretical understanding of the physical processes occurring within the sample, which result in our observations, is important in order to infer the properties of the material from the rather complex photoemission data. Two of the most popular models proposed for describing these processes are the microscopic one-step model (Feibelman and Eastman 1974) and the semiphenomenological three-step model (Spicer 1958). The one-step model is an elegant quantum mechanical approach, insofar as it treats photoemission as single wave function phenomena. The semi-classical three-step model works well for low excitation energies and is quite intuitive. The simpler three-step model has several shortcomings (*e.g.* surface effects) which the one-step model does not have. However, both models have importance in understanding the current research and will be used.

Three-step Model of Photoemission

The independent steps in the three-step model are (1) photoabsorption by a bound electron, (2) transport of that electron to the surface, and (3) its escape into the vacuum. Consequently, the photocurrent in Equation 1 factors into three parts:

$$J(E_f,h\nu) = P(E_f,h\nu)T(E_f,h\nu)D(E_f,h\nu) \qquad (2)$$

where P,T, and D are the photoabsorption, transport, and escape factors, respectively. The final energy of the photoelectron is E_f.

Figure 3 puts the three-step model in context with the notions of the solid/vacuum interface, the VB and CB density-of-states, and the three acquisition modes of photoemission. It shows a hypothetical semiconductor, analogous to GaAs, with a shallow valence band density-of-states B (*e.g.*, VBs 2,3,4 in GaAs), a deeper VB feature called C (*e.g.*, VB 1 in GaAs), and a sharp core state called D (Ga-3d). The conduction band has a abrupt edge at the conduction band minimum and various conduction band structures. Of these, feature A will be of interest here. We have taken the Fermi level to be at mid-gap as it would be for an intrinsic semiconductor. The vertical direction represents energy, whereas the horizontal takes on many connotations depending on the curve in question. To the left of the solid/vacuum interface are the processes which occur inside the solid. Those to the right, like the measurement processes, happen in the vacuum.

The photoabsorption process (step 1 in Figure 3) can occur inside the semiconductor anywhere from 60 to 300 Å below the surface (Pankove 1971), because of the relatively long photon attenuation length in the solid. An electron in an initial valence band state of energy E_i absorbs a photon of energy $h\nu$ and jumps into a final conduction band state of energy E_f. Applying this reasoning to all electrons in the B structure, produces a distribution of excited conduction band electrons called B which is identical to the valence band structure B, provided the conduction band density-of-states are not changing. The same argument applies to features C and D, however these features are not drawn in Figure 3 for clarity of presentation.

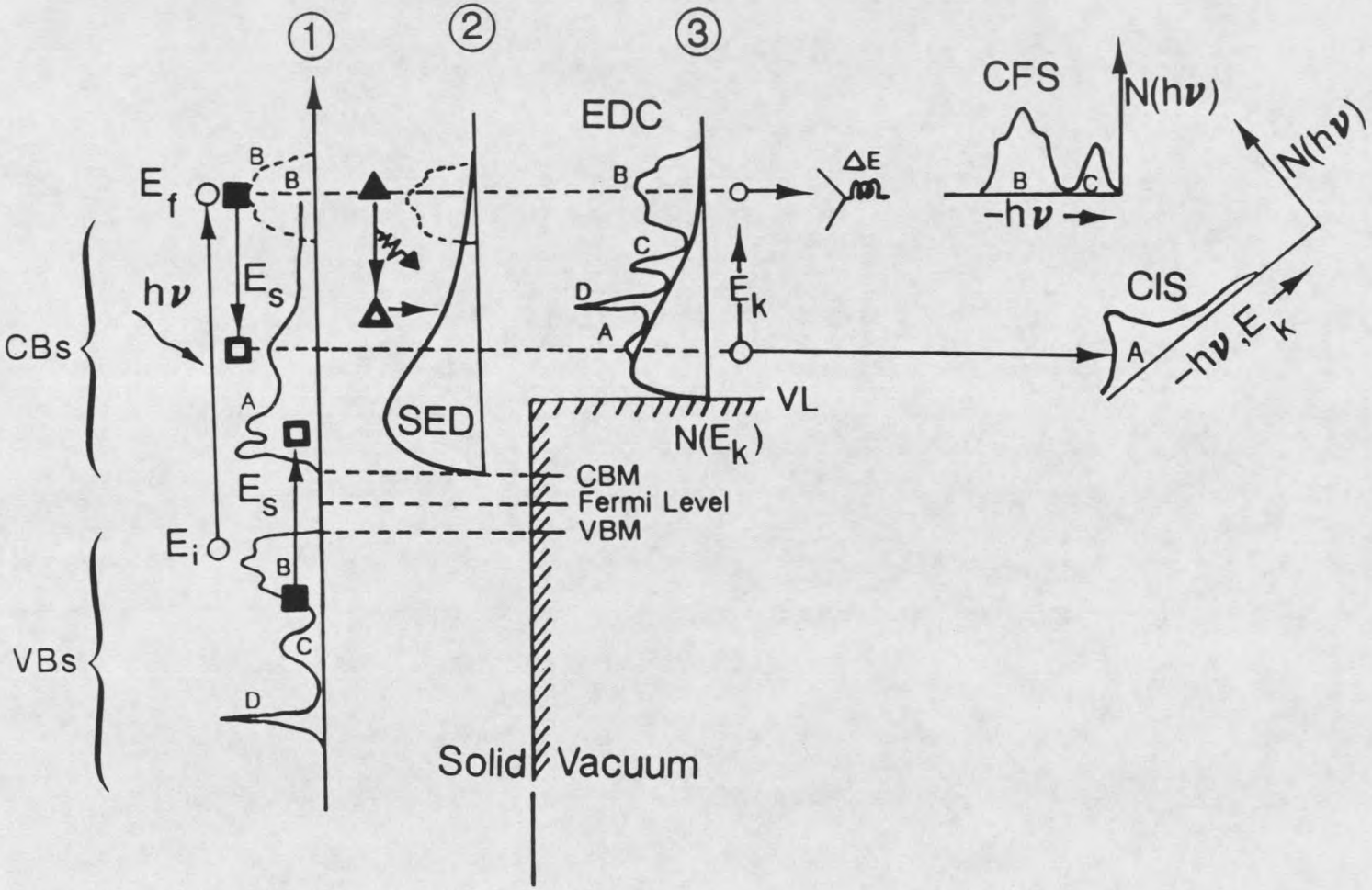

Figure 3. The three-step model of photoemission. Also shown is the relationship between the three-step model and the EDC, CFS, and CIS modes of measurement.

In a more theoretical manner, the photoabsorption factor P is derived from time-dependent perturbation theory. The effect of the photon field is represented by a time-dependent Hamiltonian $H'(t)$, which is weak compared to system's time-independent Hamiltonian H_0. Therefore, the total Hamiltonian is the summation of two:

$$H = H_0 + H'(t) \tag{3}$$

We are looking for approximate solutions to the time dependent Schrödinger equation.

$$H\Psi(\vec{r},t) = (ih/2\pi)\frac{\partial\Psi(\vec{r},t)}{\partial t} \tag{4}$$

We can write the wave function of H as a superposition of eigenfunctions $\psi_n(\vec{r})$ which are stationary states of H_0 with eigenvalues E_n (see Equation 6).

$$\Psi(\vec{r},t) = \sum c_n(t)\psi_n(\vec{r})\exp(-i2\pi E_n t/h) \tag{5}$$

$$H_0\psi_n(\vec{r}) = E_n\psi_n(\vec{r}) \tag{6}$$

Here the expansion coefficients c_n are functions of time. By substituting Equation 5 into 4 and simplifying (Saxon 1968 p.209), we obtain the time evolution of the system through the c_n's. The rate of change of these coefficients is proportional to $< \psi_f | H' | \psi_i >$, the matrix element coupling the initial state $\psi_i(\vec{r})$ to the final state $\psi_f(\vec{r})$. The transition probability that the system will go from the unperturbed initial state ψ_i to the unperturbed final state ψ_f after the interaction is $|c_n(t)|^2$.

Now let's consider the effect of an oscillating electromagnetic field in the form of a periodic perturbation (Wooten 1972, p. 109),

$$H' = \frac{V(\vec{r})}{2}\{e^{i\omega t} + e^{-i\omega t}\} \tag{7}$$